Stem Cell Reports
Resource
OPEN ACCESS

Triple S-Phase Labeling of Dividing Stem Cells

Oleg Podgorny,[1,2,3,4] Natalia Peunova,[1,2,5] June-Hee Park,[5] and Grigori Enikolopov[1,2,3,5,*]
[1]Center for Developmental Genetics
[2]Department of Anesthesiology
Stony Brook University, Stony Brook, NY 11794, USA
[3]Moscow Institute of Physics and Technology, Moscow 123182, Russian Federation
[4]Koltzov Institute of Developmental Biology RAS, Moscow 119334, Russian Federation
[5]Cold Spring Harbor Laboratory, Cold Spring Harbor, NY 11724, USA
*Correspondence: grigori.enikolopov@stonybrookmedicine.edu
https://doi.org/10.1016/j.stemcr.2017.12.020

SUMMARY

Marking replicating DNA with multiple labels presents the possibility of revealing new features and mechanisms of DNA synthesis and cell division; however, progression beyond double labeling has been hampered by cross-reactivity of label detection and scarcity of appropriate labels. Here, we present a method for triple S-phase labeling of the dividing cells, with a fourth label used to mark cells actively engaged in cell-cycle progression (e.g., using Ki67) or to phenotype the dividing cells or their progeny (e.g., using a GFP-expressing lineage reporter transgene). We apply this method to determine the parameters of neural stem cell division in the adult brain, to birth date up to four cohorts of dividing cells, and to reveal patterns of stem cell division in non-neural tissues.

INTRODUCTION

The ability to track dividing cells and determine the parameters of the cell cycle is critical to cell biology, neuroscience, and cancer research. Labeling of dividing cells with nucleotide analogs allows, among numerous applications, for measurement of cell-division kinetics, identification and tracking of subclasses of stem cells and their progeny, and evaluation of the efficacy of anticancer therapies. The use of radioactive thymidine to mark cells engaged in DNA synthesis (Hughes et al., 1958) was supplanted by the advent of halogenated nucleotides (bromo-, chloro-, or iodo-derivatives of deoxyuridine), which can be recognized with specific antibodies after their incorporation into newly synthesized DNA (Bakker et al., 1991; Gratzner, 1982). Later the DNA-labeling toolbox was expanded by the introduction of modified nucleotides that can be fluorescently tagged using click chemistry (Salic and Mitchison, 2008).

Marking the cells in the S phase of the cell cycle with two different varieties of modified nucleotides has greatly expanded the range of questions conventionally addressed using one nucleotide. Such double S-phase labeling can involve a pair of a radioactive and a halogenated nucleotide (Hayes and Nowakowski, 2002; Takahashi et al., 1994), two halogenated nucleotides that can be discriminated by antibodies (Vega and Peterson, 2005), or a pair of a halogenated and a terminal alkyne-carrying nucleotide. In addition to greatly increasing the resolution of the cell-proliferation analysis, the parallel use of two labels allows for addressing the problems that would be difficult or impossible to answer using a single type of label (e.g., cell-cycle reentry versus quiescence of dividing cells, fate of stem cell progeny, or activation of dormant cells).

It would be expected that using three (or more) types of label will bring yet another drastic increase in resolution and the ability to address an expanded range of questions. However, precise and specific resolution of three S-phase labels has not yet been achieved, primarily because of cross-reactions between antibodies and non-cognate modified nucleotides. Here, we present a method for the triple labeling of replicating DNA with modified nucleotides, with a fourth label allowing for phenotypic identification of stem cells and their progeny or additional marking of cells undergoing cell-cycle progression. We demonstrate the specificity of this technique and highlight several applications where the technique is used to investigate stem cell maintenance and division.

RESULTS

Triple-Labeling Method and Its Qualitative Validation

To label replicating DNA with three different nucleotides, we used a combination of two halogenated nucleotides (5-chloro-2′-deoxyuridine [CldU] and 5-iodo-2′-deoxyuridine [IdU]) and a terminal alkyne-bearing nucleotide (5-ethynyl-2′-deoxyuridine [EdU]), with stem and progenitor cells of various tissues marked by the expression of GFP (Nestin-GFP reporter mouse line; Mignone et al., 2004). Incorporated halogenated nucleotides were visualized using CldU-specific (rat monoclonal, clone BU1/75) and IdU-specific (mouse monoclonal, clone B44) antibodies (Vega and Peterson, 2005), and the terminal alkyne-carrying nucleotide was tracked using copper-catalyzed cycloaddition (click chemistry) with a fluorescent azide (Salic and Mitchison, 2008). We found that even with the

nucleotide-selective antibodies used under established protocols, this combination demonstrated considerable non-specific reaction between the antibodies and the incorporated EdU. We succeeded in eliminating this non-specificity by applying an additional click reaction to append a non-fluorescent azide with a bulky phenyl group. Another key improvement involved adjusting the conditions at several steps of the protocol to minimize cross-reaction between the halogenated nucleotides and the antibodies. A flow chart of the method is presented in Figure 1A and a detailed protocol is presented in Figure S1.

We first validated our method of triple S-phase labeling qualitatively, by examining the specificity of immunocytochemical and chemical reactions on the adult mouse brain sections and focusing on regions with robust neurogenesis, specifically the subventricular zone (SVZ) and the subgranular zone (SGZ) of the dentate gyrus (DG). Animals were injected with three nucleotides (CldU, IdU, and EdU) separately or in combination and each specimen was probed with antibodies and the fluorescent azide (Figure 1B). Under optimized conditions, each of the cognate pairs (anti-CldU antibody/CldU, anti-IdU antibody/IdU, and Alexa 555-azide/EdU) showed a strong signal in the sections; the non-cognate pairs (anti-CldU antibody/IdU and anti-IdU antibody/CldU) showed minimal reaction (Figures 1C and 1D); and the copper-catalyzed cycloaddition of Alexa 555-azide resulted in a robust signal only in EdU-injected specimens (Figure 1E). However, there was a significant cross-reactivity of the anti-CldU and anti-IdU antibodies (as well as a number of other available anti-5-bromo-2′-deoxyuridine [BrdU] antibodies) with the incorporated EdU moieties on the brain sections (Figure 1E), which was not eliminated by additional treatment with non-fluorescent sodium azide, prolonged click reaction, or increased concentration of the fluorescent azide (not shown). To suppress the non-specific signal, we have chosen, among other azides, the azidomethyl phenyl sulfide (Liboska et al., 2012) for treatment of the sections after the reaction with the fluorescent azide and before incubation with antibodies. Such pretreatment eliminated the non-specific reaction of the incorporated EdU with the antibodies, while preserving its reaction with the fluorescent Alexa 555-azide (Figure 1F).

As an additional test for the specificity of reaction, we analyzed the labeled nuclei on the brain sections from animals that received all three labels sequentially: a single injection of EdU, followed by single injections of CldU, and then a final injection of IdU, each separated by 2 hr, and all animals were sacrificed 2 hr after the last injection (Figure 1B) (in these experiments we focused on the SVZ, which contains significantly more dividing cells than the SGZ). Since the S phase, as well as the interval between two S phases of the dividing cells in the adult SVZ, is over 6 hr (Ponti et al., 2013), it would be expected that nuclei with all combinations of incorporated nucleotides could be detected, except for populations of cells labeled only with CldU ($CldU^{+}_{only}$ cells) (because CldU incorporation is expected to be either preceded by EdU incorporation or followed by IdU incorporation) and of $EdU^{+}IdU^{+}_{only}$ cells (because injected CldU is expected to incorporate into DNA within the 4 hr interval between the EdU and the IdU injections). Indeed, we found nuclei stained for EdU^{+}_{only}, IdU^{+}_{only}, $EdU^{+}CldU^{+}$, $CldU^{+}IdU^{+}$, and $EdU^{+}CldU^{+}IdU^{+}$, but not for $EdU^{+}IdU^{+}$ or $CldU^{+}_{only}$ (Figures 1G and 1H), confirming the specificity of the nucleotide detection. Notably, with sequentially injected multiple labels, EdU, CldU, and IdU signals showed different spatial distributions in the nuclei (Figure 1H); this may reflect the fact that various regions of the genome are replicating at different times of the S phase and are packed and distributed differentially in the nucleus.

Quantitative Validation of the Method and Determination of the S-Phase Length

We next evaluated the quantitative aspects of our triple S-phase labeling method, by injecting Nestin-GFP animals with CldU, EdU, and IdU sequentially with 2 hr intervals between introduction of the labels and analyzing the brains 2 hr after the last injection. In these series we focused on the SGZ of the DG because the dividing GFP-expressing stem and progenitor cells of the DG do not migrate away from the SGZ within the time frame of our experiments and therefore can be accurately quantified.

Labeled stem and progenitor cells can be precisely identified and phenotyped using the three nucleotide labels in combination with the Nestin-GFP reporter transgene (Figure 2). Progenitor cells in the adult SGZ are a fairly homogeneous population with regard to the length of the cell cycle and the S phase (Encinas et al., 2011; Hayes and Nowakowski, 2002; Nowakowski et al., 1989). Therefore, sequentially injected labels mark the linear progression of the cycling cells through the S phase (note that for quantitative equivalency the doses of all injected nucleotide analogs must be equimolar; Vega and Peterson, 2005), so that defined numbers and types of labeled cells can be expected (Figure 2A). First, the numbers of GFP-expressing SGZ cells labeled with each nucleotide are expected to be similar because the bulk of the cells are not expected to pass through mitosis and duplicate within the 2–6 hr interval between label injection and analysis. Second, the numbers of $CldU^{+}_{only}$, $CldU^{+}EdU^{+}_{only}$, $EdU^{+}IdU^{+}_{only}$, and IdU^{+}_{only} cells must be similar and lower than that of $CldU^{+}EdU^{+}IdU^{+}$ cells, because the former four groups correspond to the fractions of populations that have left or entered the S phase within each 2 hr interval. Third, with the S phase and total cell-cycle duration exceeding 4 hr, detection of

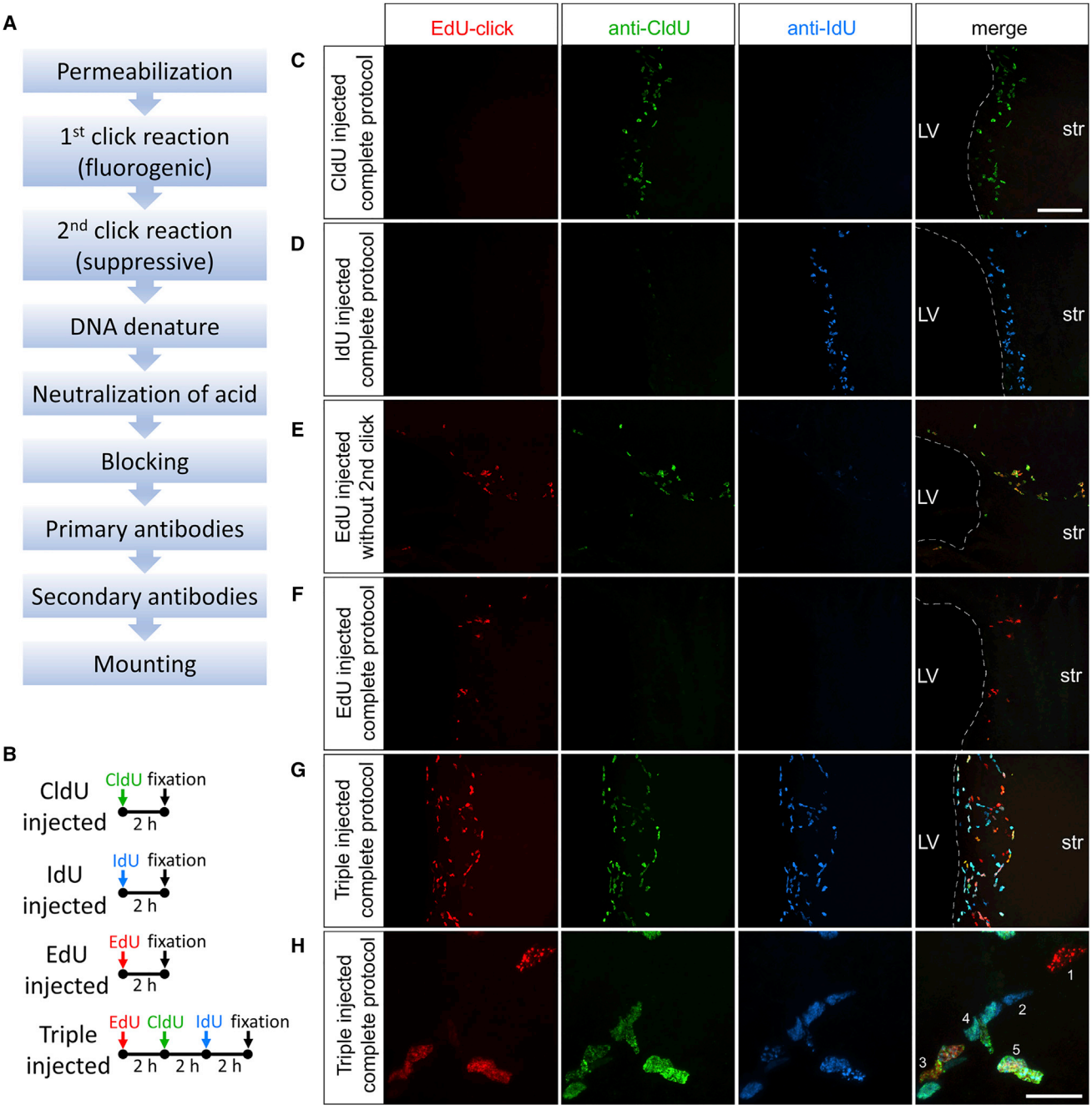

Figure 1. Qualitative Validation of Triple S-Phase Labeling of Neural Stem and Progenitor Cells

(A) The workflow of staining. The critical step is the suppressive second click reaction for eliminating non-specific antibody binding to non-reacted EdU. A detailed protocol of staining is presented in Figure S1.

(B) Labeling paradigm. Mice received injections of three nucleotides (CldU, IdU, and EdU) separately or in combination.

(C–H) SVZ of mice that received CldU, IdU, and EdU injections separately or in combination. (C and D) Complete protocol of staining produces a strong signal by the respective cognate pairs: anti-CldU antibody/CldU (C) and anti-IdU antibody/IdU (D). (E) Click reaction produces strong signal only in the EdU-injected mouse; however, there is also significant non-specific binding of anti-CldU and anti-IdU antibodies to EdU. (F) Suppressive second click reaction eliminates non-specific binding of antibodies to EdU. (G and H) Only the expected combinations of labels are detected in triple-injected mouse: EdU_{only} (1), IdU_{only} (2), $EdU^{+}CldU^{+}$ (3), $CldU^{+}IdU^{+}$ (4), and $EdU^{+}CldU^{+}IdU^{+}$ (5). Data presented in (C–G) were confirmed by spectral imaging (for details see Supplemental Experimental Procedures and Figure S3). LV, lateral ventricle; str, striatum. Scale bars: (C) 100 μm (the same scale bar for D–G), (H) 20 μm.

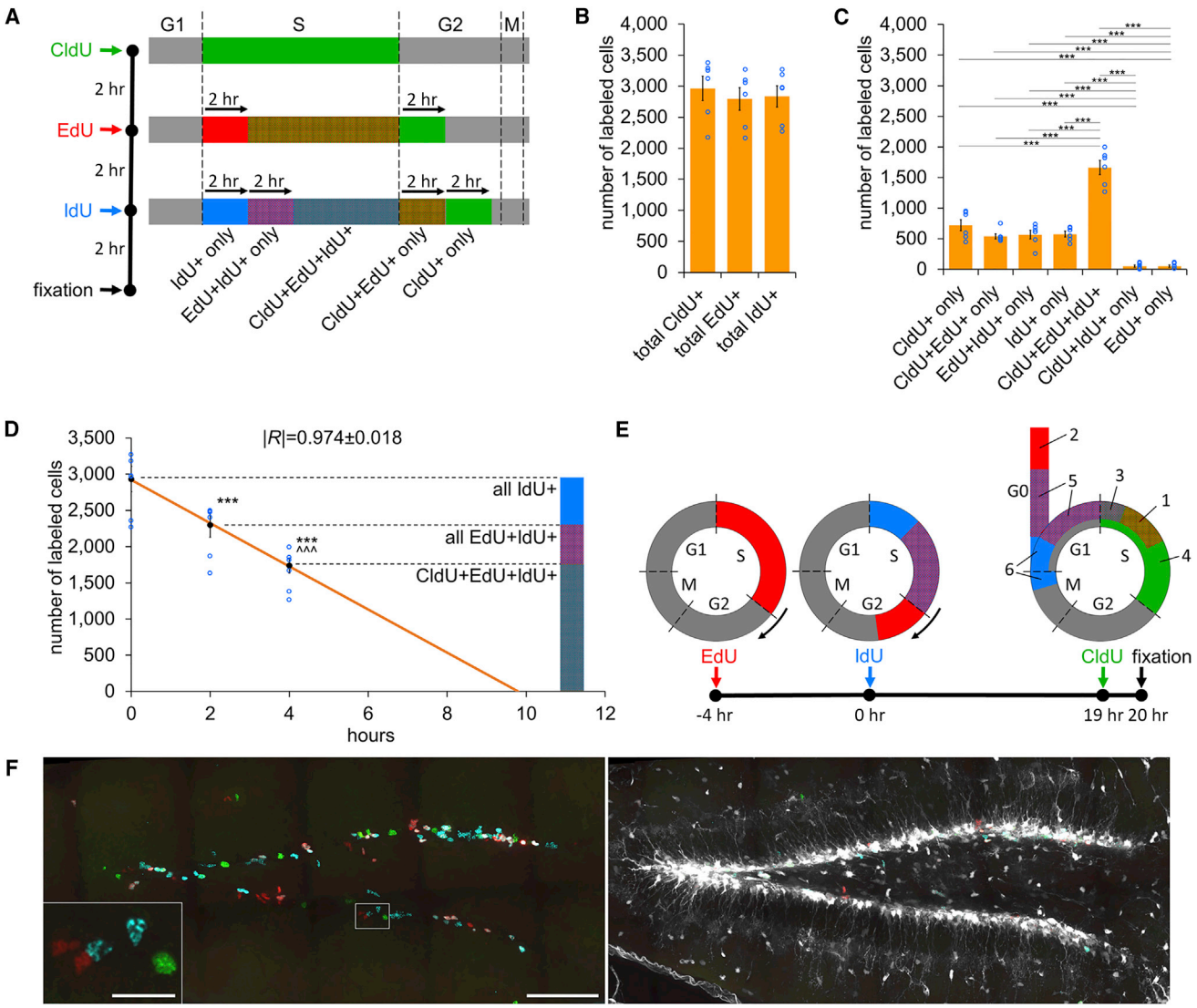

Figure 2. Quantitative Validation of Triple S-Phase Labeling and Determination of Neural Stem and Progenitor Cells Reentry into the Cell Cycle

(A) Labeling paradigm and representation of progression of sequentially labeled cells through the cell cycle. Defined numbers and types of labeled cells can be expected according to the hypothetical linear progression of neural progenitors through the cell cycle.

(B) Numbers of cells that have incorporated each nucleotide under the labeling paradigm presented in (A). n = 6 mice.

(C) Numbers of cells that have incorporated different combinations of three nucleotides under the labeling paradigm presented in (A). n = 6 mice, ***p < 0.001.

(D) A linear decrease of all IdU-positive cells (which include the IdU^{+}_{only}, $EdU^{+}IdU^{+}_{only}$, and $CldU^{+}EdU^{+}IdU^{+}$ cell subpopulations, color encoded as in A), all $EdU^{+}IdU^{+}$ cells (which include the $EdU^{+}IdU^{+}_{only}$ and $CldU^{+}EdU^{+}IdU^{+}$ subpopulations), and $CldU^{+}EdU^{+}IdU^{+}$ cells in relation to the time intervals between nucleotide injections under the labeling paradigm presented in (A). The x-axis intercept of the regression line provides an estimation of the S-phase length. n = 6 mice, ***p < 0.001 in comparison with all IdU-positive, ^^^p < 0.001 in comparison with all $EdU^{+}IdU^{+}$ cells.

(E) Labeling paradigm for the determination of the cell-cycle reentry and cell-cycle diagrams showing progression of labeled cells through the cell cycle. Six combinations of three labels were expected under this paradigm: $EdU^{+}CldU^{+}_{only}$ (1), EdU^{+}_{only} (2), $CldU^{+}EdU^{+}IdU^{+}$ (3), $CldU^{+}_{only}$ (4), $EdU^{+}IdU^{+}_{only}$ (5), and IdU^{+}_{only} (6). Gray color shows population of all cycling cells that have not incorporated any label. Defined numbers and types of labeled cells can be expected in this paradigm (see text for details).

(F) Pseudocolored (EdU, red; IdU, cyan; CldU, green; and GFP, white) representative image of the Nestin-GFP DG labeled as described in (E). The left shows the same area as the right but without the GFP channel. Inset shows closely positioned cells that incorporated individual labels, confirming the specificity of our protocol. Scale bar, 100 μm; in the inset, 20 μm. Quantitative data are presented as mean ± SEM.

EdU^+_{only} and $CldU^+IdU^+$ cells is not expected for the reasons described above. Finally, the numbers for all IdU-positive cells (which include the IdU^+_{only}, $EdU^+IdU^+_{only}$, and $CldU^+EdU^+IdU^+$ cell subpopulations), all EdU^+IdU^+ cells (which include the $EdU^+IdU^+_{only}$ and $CldU^+EdU^+IdU^+$ subpopulations), and $CldU^+EdU^+IdU^+$ cells should decrease linearly, because they reflect the fractions of cells remaining in the S phase at the time of IdU injection (i.e., with CldU- and EdU-labeled cells gradually leaving the S phase).

Quantification of the GFP-expressing nucleotide-labeled cell subpopulations in the DG conformed to these expectations (Figures 2B and 2C). The numbers of cells with each of the three labels were similar (a non-significant increase in the number of CldU-labeled cells may reflect mitosis and duplication of the fraction of cells that were close to exiting the S phase at the time of CldU injection) (Figure 2B). The size of the $CldU^+_{only}$, $CldU^+EdU^+_{only}$, $EdU^+IdU^+_{only}$, and IdU^+_{only} subpopulations did not differ and was lower than that of the $CldU^+EdU^+IdU^+$ population. Furthermore, the number of cells with the unlikely combinations (EdU^+_{only} and $CldU^+IdU^+$) was negligible (Figure 2C). Finally, the numbers of IdU^+, EdU^+IdU^+, and $CldU^+EdU^+IdU^+$ cells showed a linear decrease with a regression coefficient of 0.974 ± 0.018 (Figure 2D). The x-axis intercept of the regression line corresponds to the duration of the S phase and defines it for these experiments as 9.8 ± 0.2 hr.

Application: Reentry into the Cell Cycle

Cell-cycle reentry, defined as the percentage of cycling cells that remain in the cell cycle after mitosis, is an important parameter of cell-proliferation kinetics. It can be estimated by labeling the cells with two labels within a time interval equal to the cell-cycle length. However, even modest variability in the length of the cell cycle may result in an underestimation of the true reentry value. This limitation of the method was overcome by a double-labeling paradigm that uses two separate groups of animals to determine the fraction of cells that exit or remain in the cell cycle (Takahashi et al., 1994, 1995, 1996). We asked whether our triple-label approach could be employed to determine this parameter within the same group of animals. Assuming that the approximate lengths of the cell cycle (T_C) and of the S phase (T_S) are 28 and 10 hr, respectively (Encinas et al., 2011 and Figure 2D), we developed a labeling paradigm where Nestin-GFP reporter animals were injected with EdU at a −4 hr time point and with IdU at the time point of 0 hr (Figures 2E and 2F). This defines a "4 hr cohort" of cells with known position in the cell cycle. The cohort is expected to be traversing the S phase within the time interval from T_C-T_S to T_C-4 hr. Therefore, if the third label (CldU) is injected within the 18–24 hr time interval after the second label (19 hr in our experiment), $EdU^+CldU^+_{only}$ cells correspond to the cells of the 4 hr cohort that have undergone an additional S phase, whereas the EdU^+_{only} cells represent cells that have left the cell cycle after mitosis (Figure 2E). Therefore, cell-cycle reentry (CCR) can be determined as

$$\mathrm{CCR}\ (\%) = \frac{N_1}{(N_1 + N_2)/2} \times 100\ , \qquad \text{(Equation 1)}$$

where N_1 is the number of $EdU^+CldU^+_{only}$ cells (population 1 in Figure 2E) and N_2 equals the number of EdU^+_{only} cells (population 2 in Figure 2E). The denominator in the equation is halved because N_1 + N_2 corresponds to the 4 hr cohort of cells after doubling. We determined the number of cells in N_1 as 575 ± 65 and in N_2 as 897 ± 108, which indicates a CCR rate of 78.3% ± 5.6%. This corresponds to approximately four divisions undergone by stem and progenitor cells if they are engaged into symmetric divisions and less if a fraction of them undergo asymmetric divisions.

These labeling experiments provide additional evidence for the specificity of the method. First, certain combinations of the probes and the numbers of labeled cells are expected in the paradigm presented in Figure 2E. According to the cell-cycle diagram in Figure 2E, all cells labeled with EdU (sum of populations 1, 2, 3, and 5) and the bulk of cells labeled with IdU (sum of populations 3, 5, and 6) are expected to traverse the mitotic division. Therefore, the total number of cells labeled individually with EdU or IdU is expected to be twice that of the total number of cells labeled individually with CldU (sum of populations 1, 3, and 4). Indeed, we found that the total numbers of DG cells labeled individually with EdU or IdU was 2-fold higher than that of CldU-labeled cells (3,742 ± 276 and 3,568 ± 229 versus 1,830 ± 172, respectively; n = 6 mice, $p < 0.001$). Second, the absence of triple-labeled cells (population 3) would indicate that not all cycling cells from the 4 hr cohort (population 1) have reached the next S phase, whereas more than 1.5-fold increase of triple-labeled cells over the cycling cells of the 4 hr cohort would indicate that some of the cycling cells from the 4 hr cohort have finished the next S phase and reached the G2 phase at the time of CldU injection; i.e., we would expect the population 3/population 1 ratio to be more than 0 and less than 1.5. Our experimental data (330 ± 33 cells for population 3 and 575 ± 65 cells for population 1, ratio = 0.57) conform to the notion that all cycling cells from the 4 hr cohort were in the S phase at the time of CldU injection. Finally, populations of cells labeled with IdU_{only} and $CldU_{only}$ are not expected in this labeling paradigm, and, indeed, we detected a negligible number of such cells (40 ± 12 per entire DG; potentially, this may be due to a small subpopulation of cells with distinct S-phase and cell-cycle lengths or to residual cross-reaction between the anti-CldU and the anti-IdU antibodies).

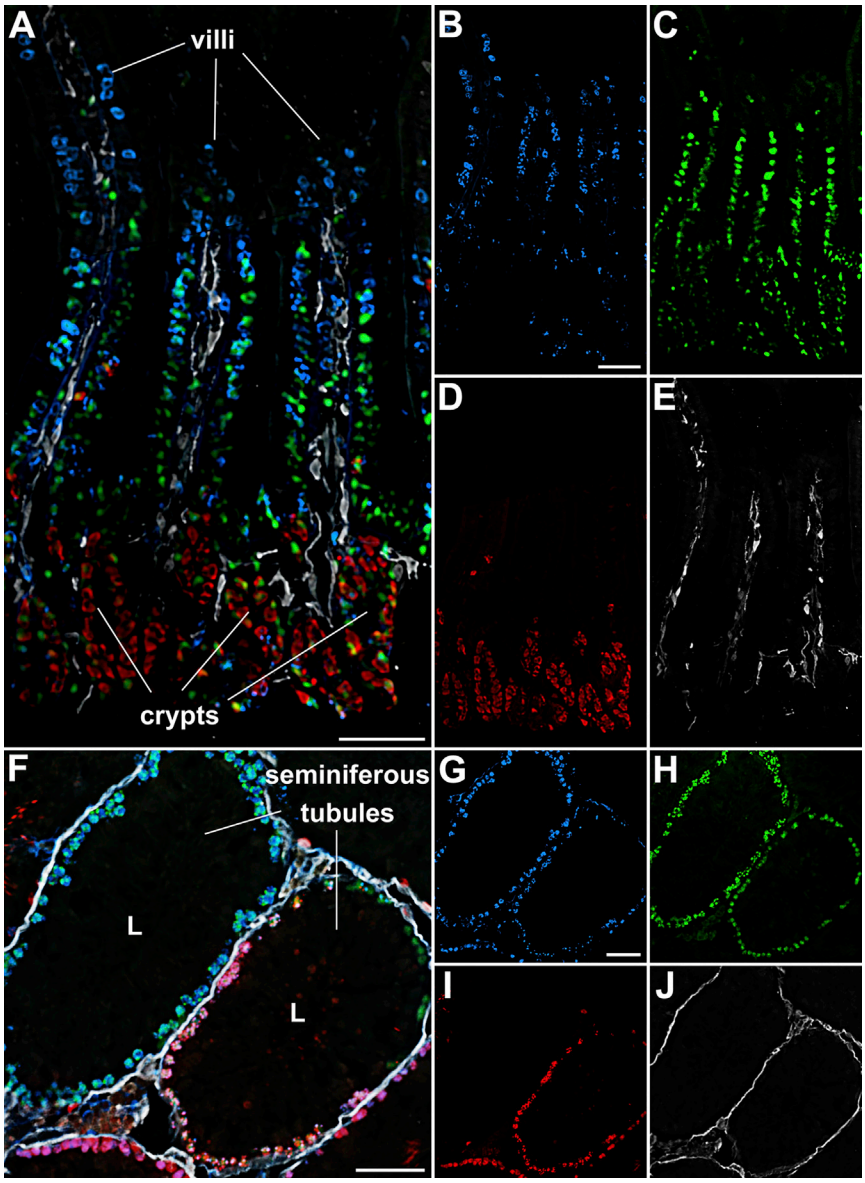

Figure 3. Triple S-Phase Labeling of Stem Cells in Rapidly Renewing Tissues

(A) Pseudocolored (IdU, cyan; CldU, green; EdU, red; and GFP, white) representative images of sections of Nestin-GFP mouse intestine after sequential injection of IdU, CldU, and EdU every 24 hr.

(B–E) Separate channel representation of (A). (B) IdU, (C) CldU, (D) EdU, (E) GFP. Note the segregation of defined cell populations at different stages of differentiation, as they ascend from the crypts along the villi.

(F) Pseudocolored (IdU, cyan; CldU, green; EdU, red; and GFP, white) representative images of sections of Nestin-GFP mouse seminiferous tubules after sequential injection of IdU, CldU, and EdU every 24 hr.

(G–J) Separate channel representation of (F). (G) IdU, (H) CldU, (I) EdU, (J) GFP. Note that profiles of individual tubules show defined cell populations at different stages of differentiation, including those with one, two, or three labels. L, lumen of seminiferous tubule.

Scale bars, 50 μm.

Applications: Division of Stem and Progenitor Cells

To demonstrate the utility of our method for studying various types of stem cells, we applied it to several tissues that undergo extensive self-renewal and whose anatomy allows for the unambiguous identification of dividing stem cells and their progeny. We injected Nestin-GFP mice with IdU, followed in 24 hr by CldU and in 48 hr by EdU, and then analyzed the tissues 2 hr after the last injection.

Mammalian Intestinal Stem Cells

Differentiated enterocytes in the intestine arise from stem cells located in the crypts. These cells are engaged in rapid self-renewing divisions, giving rise to progeny, which rapidly divides, differentiates, and undergoes apoptosis, all the while rapidly ascending along the surface of the villi to the top where apoptotic cells are shed into the lumen 4–5 days after they are born (Clevers, 2013). The bottom-tip flow of cells, revealed as clonal ribbons, is particularly well suited for analyzing the division kinetics and patterns of intestinal stem and progenitor cells.

Triple S-phase labeling (IdU, CldU, and EdU injected sequentially every 24 hr, with the tissues analyzed 2 hr after the last injection) reveals all subtypes of labeled cells in the intestine in different compartments, with the fourth label (GFP) primarily marking perivascular cells (Kulkarni et al., 2017) and highlighting the anatomy of the villi (Figures 3A–3E). We observed all expected combinations of labels: IdU^{+}_{only}, $CldU^{+}_{only}$, EdU^{+}_{only}, $IdU^{+}CldU^{+}$, $IdU^{+}EdU^{+}$, $CldU^{+}EdU^{+}$, and rare cells with all three labels. Consistent

with the expected kinetics of division, differentiation, and migration, we observed only IdU-labeled cells at the top of the villi; only IdU, CldU, and IdU/CldU-labeled cells in the middle of the villi; and mainly EdU-labeled cells in the crypts, with some IdU- and CldU-labeled cells detected in the crypts. IdU^{+}_{only} cells correspond to the most differentiated stem cell progeny with the earliest birth date, with some having reached the tip of the villi to be soon shed off the tip. $CldU^{+}_{only}$ cells correspond to differentiated cells born 26 hr ago, which are leaving the proliferative crypt zone. $IdU^{+}CldU^{+}$ cells correspond to cells born 50 hr ago, which were still cycling at the time of CldU injection. EdU^{+} cells mainly correspond to the transiently amplifying progenitor cells of the crypt that cease to divide upon leaving the crypt. Finally, the double- and triple-labeled cells of the crypt may correspond to the transit-amplifying progenitors and, in the lower aspects of the crypt, to crypt base columnar cells that act as the self-renewing stem cells of the intestinal epithelium. These patterns are fully consistent with the known sequence of events during the enterocyte's life cycle (Clevers, 2013), with triple labeling revealing the clearly defined stages in the conveyor belt pattern of division and migration, the sharp boundaries of the crypt proliferative zone, and the defined populations of self-renewing stem and progenitor cells; a detailed kinetic analysis (e.g., with multiple time points) would determine the parameters of the division/differentiation progression of the intestinal stem cells with high precision.

Mammalian Seminiferous Tubules

Mammalian spermatogenesis proceeds through well-defined stages of division of spermatogonia that are gradually converted into postmeiotic spermatids (Griswold, 2016; Oatley and Brinster, 2012). Triple S-phase labeling (the same labeling scheme as used for the intestinal stem cells) demonstrates the presence of dividing cells with all expected combinations of labels (Figures 3F–3J). It also shows that waves of division and differentiation in the adjacent tubules are not closely coordinated such that the combinations of labels on the neighboring tubules' profiles rarely match. As with the intestinal stem cells, a detailed kinetic analysis of label inclusion in the testis may reveal complex and non-obvious patterns of coordination of division and migration across the tissue, parameters of progenitor cell division, and self-renewal or interconversion of stem cells and their more advanced progeny.

Quadruple Labeling of Cycling Cell Subpopulations

While endogenous or exogenous lineage markers (such as Nestin-GFP reporter in the experiments above) allow for phenotyping the dividing cells, it may be advantageous in certain experimental settings to introduce yet another marker of cell division to mark additional cohorts of dividing cells. We combined the labeling paradigm described above (IdU, CldU, and EdU injections 24 hr apart, with the analysis 2 hr after the last label injection) with visualizing cells engaged in division cycle at the time of analysis using antibody to Ki67, a marker of cells undergoing cell-cycle transit. In both the SVZ and the SGZ, cells with the expected combinations of labels were evident (Figures 4A, 4B, and 4D–4H), revealing four separate cohorts of neural progenitors (with the Ki67 and EdU signals largely overlapping, as expected). The advantage of quadruple cell division labeling was particularly evident in the specimens of intestine where four signals revealed the rapid migration of new cells from the crypts to the top of the villi: IdU^{+} cells at the top of the villi, $CldU^{+}$ cells in the middle segment of the villi, EdU^{+} cells strictly in the crypts, and $Ki67^{+}$ cells in the crypts and the basal segment of the villi (Figures 4C and 4I–4M). As expected, $CldU^{+}$ cells partially overlapped with IdU-, EdU-, and Ki67-labeled cells, reflecting the rapid time course of enterocytes' ascent from the crypts to the top of the villi. Also, as expected, we were able to detect quadruple-labeled nuclei with a characteristic morphology of Lgr5-expressing stem cells of the intestine (Figures 4I–4M).

Together, these three examples (brain, intestine, and testis) highlight the features of the stem cell's life cycle that our method can reveal. These features would have previously been difficult or impossible to detect using single or double S-phase labeling.

DISCUSSION

Here, we present a method for multilabel analysis of division and differentiation of stem cells and their progeny. Quadruple labeling, with GFP highlighting stem and progenitor cells, allows for the unambiguous identification of cells that have undergone single or multiple rounds of DNA replication. A modification of this approach, with the Ki67 marker of active cell proliferation added to the detection protocol, allows for the quadruple labeling of dividing cell populations.

The key features and advantages of our method include multiple birth dating of up to four cohorts and multiple subpopulations of dividing cells; parallel analysis of cell division, cell-cycle reentering, and differentiation in the same organism or tissue specimen and in a specified cell type (identified through additional endogenous or exogenous lineage markers, analogous to Nestin-GFP reporter); increased precision of quantitative analysis of the main kinetic parameters of cell division in animals or cells; and combination of different labeling paradigms, such as pulse chase and cumulative labeling, within the same animal or specimen. Overall, this method expands the range of questions regarding cell maintenance, division, and differentiation. We verified the method qualitatively, demonstrating

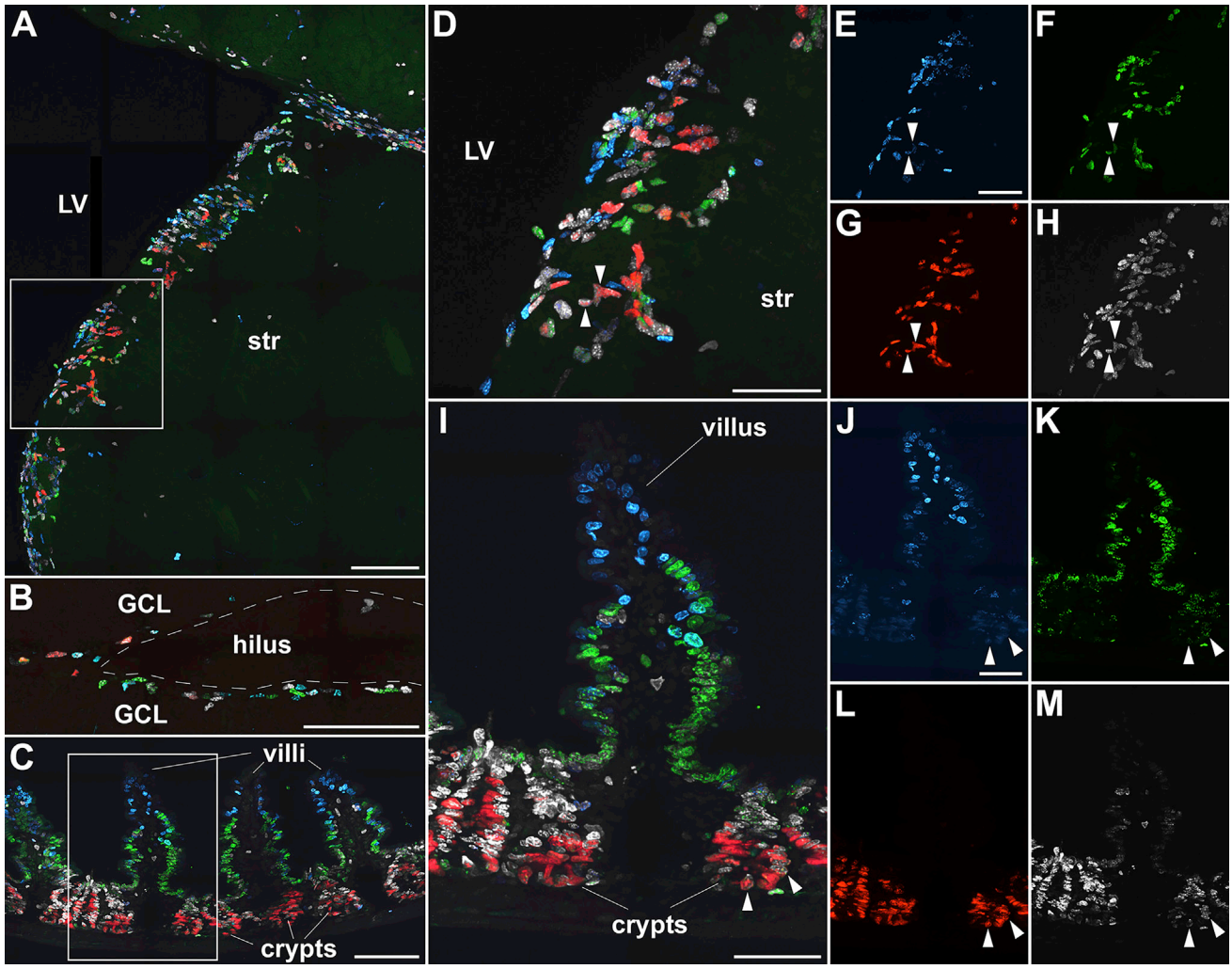

Figure 4. Quadruple Labeling of Cycling Cell Cohorts in the Brain and Intestine of C57BL/6 Mouse

(A–C) Pseudocolored (IdU, cyan; CldU, green; EdU, red; and Ki67, white) representative images of the SVZ (A), DG (B), and intestine (C) of C57BL/6 mouse after sequential injection of IdU, CldU, and EdU every 24 hr.

(D) Detailed representation of the area in (A) confined by the rectangular frame.

(E–H) Separate channel representation of (D). (E) IdU, (F) CldU, (G) EdU, (H) Ki67. Arrowheads indicate the cells that have incorporated all three labels and are also co-stained with Ki67 antibody.

(I) Detailed representation of the area in (C) confined by the rectangular frame.

(J–M) Separate channel representation of (I). (J) IdU, (K) CldU, (L) EdU, (M) Ki67.

Arrowheads indicate the cells that have incorporated all three labels and are also co-stained with Ki67 antibody. Note that in these experiments staining was performed with a modified protocol to eliminate non-specific binding of the secondary anti-mouse IgG antibody (for details see Figure S2). LV, lateral ventricle; str, striatum; GCL, granular cell layer of the DG. Scale bars: (A–C) 100 μm, (D–M) 50 μm.

minimal cross-reactivity between different labels, which compromised previous attempts. We verified the method quantitatively, demonstrating full agreement with the predicted parameters of the labeling reactions and kinetics. We demonstrated the utility of the method by determining with increased precision the length of the S phase in the dividing progenitor population of the DG. We further demonstrated the utility of our method by determining the fraction of dividing neural progenitors that reenter the cell cycle, a parameter important for determining the modes of division of stem cells and their progeny. Furthermore, we used this method to reveal stages of stem and progenitor cell division in the intestine and in seminiferous tubules.

Our method will help to reveal new features of maintenance and division of stem cells and of cancer cells or to ascertain previously known parameters with increased precision. The combinatorial nature of multiple labeling allows for following over a dozen stem and progenitor cell

subpopulations. It allows for combination of different labeling paradigms, such as pulse chase and cumulative labeling, within the same animals or specimens, to investigate complex features of proliferating cells, such as distinct steps of their cell-cycle entry or exit, elimination, or differentiation. It will also decrease the effort and cost of complex stem cell analysis, allowing parallel estimations of proliferation, CCR, differentiation, and cell elimination within the same experiment, the same animal, and the same specimen. Importantly, this method can be further expanded to accommodate additional DNA and cell-type labels.

Along with the advantages of this method, there are several caveats to consider when applying the triple S-phase labeling technique. First, the bioavailability and pharmacokinetics of each of three nucleotides in animals have not been precisely determined (although note that we detect the same numbers of labeled stem and progenitor cells in the brain after injecting each of those compounds, which argues against significant differences between nucleotides' bioavailability; Figure 2B). This may not be critical when injection of the labels is separated by hours and days (provided that the label concentrations are close to saturating), but may affect the results and the conclusions if the injections are spaced too closely (e.g., separated by minutes). Second, long-term stability of the nucleotide modifications, once they are incorporated into the DNA, has not been thoroughly investigated. It is conceivable that metabolism or repair-directed mechanisms may modify the nucleotides or remove critical groups (consider that certain bacterial species have active dehalogenating systems). While the modifications appear to be stable in the short term (the same number of labeled neurons can be detected at different time intervals after pulse labeling), longer term (months and years) stability, even for BrdU, has not been critically evaluated. Third, modified nucleotides themselves may distort the process of DNA duplication or cell division, differentiation, and maintenance. There is accumulating evidence that EdU, in particular, may affect cell viability or division at high concentrations (Kohlmeier et al., 2013; Ponti et al., 2013). Therefore, a proper concentration window may need to be determined for these or yet to come modified analogs. Fourth, while our protocol ensures minimal overlap between the antibody- or azide-guided detection of each nucleotide, this overlap may vary for different antibodies and has to be systematically determined and carefully controlled. Finally, with the expanded range of methods for preparing and clarifying neural and other tissues (Treweek and Gradinaru, 2016; Yang et al., 2014), which of the whole-mount imaging techniques are most compatible with our quadruple-labeling protocol remains to be determined.

In sum, our method increases the resolution and range of cycle analysis and offers access to a range of questions that have so far been difficult or impossible to address. Further expansion of the range of available nucleotide analogs, fluorescent labels, and cell-type-specific reporters is required to increase the resolution of the cell cycle and stem cell fate analysis and the range of stem cells, tissues, and processes that can be analyzed.

EXPERIMENTAL PROCEDURES

Animals

Experiments were conducted using C57BL/6 (The Jackson Laboratory) and Nestin-GFP transgenic mice (Mignone et al., 2004). Mice were group housed (maximum four per cage) in an animal facility approved by the Association for the Assessment and Accreditation of Laboratory Animal Care International (AAALAC) at Stony Brook University in a temperature-controlled (22°C) room with a 12 hr light/dark cycle (lights from 7:00 a.m. to 7:00 p.m.) and free access to food and water. All experimental procedures were approved by the Stony Brook University Animal Use Committee and performed according to the NIH guidelines.

Qualitative Validation of Triple-Labeling Method

To demonstrate specificity of our protocol for the visualization of three thymidine analogs, four 5-month-old C57BL/6 males were either injected with a single thymidine analog, CldU (Sigma-Aldrich) at a dose of 128 mg/kg with the final concentration of 6.4 mg/mL, IdU (Sigma-Aldrich) at a dose of 173 mg/kg with the final concentration of 2.47 mg/mL, or EdU (Life Technologies) at a dose 123 mg/kg with the final concentration of 6.15 mg/mL, or sequentially injected with EdU, CldU, and IdU at the same doses and final concentrations at 2 hr intervals (Figure 1B). The animals were deeply anesthetized and perfused 2 hr after receiving the injections or, for the sequential injection, 2 hr after the last injection.

All compounds were dissolved in sterile PBS (pH 7.4, Fisher Scientific). The doses of the thymidine analogs were equimolar to the saturating dose of 150 mg/kg BrdU, which was shown to label the maximal number of cells in the S phase in the DG of the hippocampus after a single injection (Mandyam et al., 2007).

Quantitative Validation of Triple-Labeling Method

To confirm the equivalent labeling capacity of all three thymidine analogs, we used the triple-labeling method to estimate the duration of the S phase of neural progenitors' cell cycle in the DG and compared the results with the previous data obtained in the double-labeling experiments. Six Nestin-GFP mice (2-month-old females) received sequential injections of CldU, EdU, and IdU at the same doses and final concentrations as described above, at 2 hr intervals (Figure 2A), and were deeply anesthetized and perfused 2 hr after last injection.

Determination of Cell-Cycle Reentry

To determine the true value of CCR, we injected six Nestin-GFP mice (2-month-old males) with EdU, IdU, and CldU at time points −4, 0, and 19 hr, respectively (Figure 2E). Thymidine analogs were injected at the same doses and final concentrations as above and the animals were deeply anesthetized and perfused 1 hr after the last injection.

Triple-Labeling Method for Visualization of Several Cohorts of Proliferating Cells in Various Tissues

To illustrate the applicability of the triple labeling to various tissues, Nestin-GFP mice (2-month-old males) and C57BL/6 mice (2.5-month-old males) received sequential injections of IdU, CldU, and EdU at the same doses and final concentrations as above with 24 hr intervals and were deeply anesthetized and perfused 2 hr after the last injection.

Perfusion of Mice and Tissue Processing

All mice were deeply anesthetized with 400 μL of 15% chloral hydrate (Sigma-Aldrich) in sterile PBS prior perfusion. Animals were then transcardially perfused with PBS followed by perfusion with chilled 4% paraformaldehyde in PBS. Brain and testis were procured and postfixed overnight in 4% paraformaldehyde in PBS at 4°C. To obtain intestine preparations, an ~1 cm long piece of the gut was cut from a deeply anesthetized animal before the transcardial perfusion. The piece of the gut was washed of feces in PBS, followed by overnight fixation in 4% paraformaldehyde in PBS at 4°C.

After overnight postfixation, all tissues were washed with PBS. Brains were immediately used for the vibratome sectioning. Right hemispheres were sectioned sagittally and 50 μm sections were collected sequentially in 6 wells of a 24 well plate in such manner that each well contained in series every sixth section of the entire hemisphere (Encinas and Enikolopov, 2008). Other tissues were placed in 30% sucrose at 4°C overnight followed by cryosectioning. Ten micrometer cryosections were placed on Superfrost Plus glass slides.

Visualization of Three Thymidine Analogs in C57BL/6 and Nestin-GFP Mice

Free-floating brain sections were stained in the wells of a 24 well plate. Cryosections attached to glass slides were circumscribed with a hydrophobic barrier pen and the staining was performed in a droplet in the humid chamber. The volumes of the click reactions and the primary and secondary antibody reactions were 500 and 150 μL for the free-floating brain sections and the attached testis and gut cryosections, respectively. All procedures were performed at room temperature except for DNA denaturation (see below).

Sections were initially permeabilized in 4% Triton X-100 (Sigma-Aldrich) in PBS for 1 hr with subsequent washing in PBS for three times. Then the first click reaction was performed for EdU visualization. The first click reaction included 20 mM (+)-sodium L-ascorbate (Sigma-Aldrich), 10 μM Alexa 555-azide (Life Technologies), and 4 mM copper sulfate (Sigma-Aldrich) in PBS. Sections were incubated in the solution with gentle shaking for 15 min followed by three washings in PBS. The second click reaction was performed to suppress unwanted cross-reactivity of the anti-CldU and anti-IdU antibodies (see below) to those EdU nucleotides that remained unoccupied by Alexa 555-azide after the first click reaction. For the second click reaction, we used azidomethyl phenyl sulfide, which is known to suppress cross-reactivity of different anti-BrdU antibodies to EdU (Liboska et al., 2012). The solution for the second click reaction included 20 mM (+)-sodium L-ascorbate, 2 mM azidomethyl phenyl sulfide (Sigma-Aldrich), and 4 mM copper sulfate in PBS. Sections were incubated in the solution with gentle shaking for 15 min and subsequently washed three times in PBS.

To denature DNA, sections were incubated in 2 N hydrochloric acid at 37°C for 40 min. Then hydrochloric acid was neutralized by incubating the sections with 0.1 M borate (pH 8.0) twice for 10 min. After three consequent washes with PBS, sections were blocked with 5% normal goat serum (Sigma-Aldrich) in PBS containing 0.1% Triton X-100 (PBST) for 1 hr. The blocking solution was replaced with 5% normal goat serum in PBST containing primary rat monoclonal anti-CldU antibody at a dilution 1:1,000 (clone BU1/75, Accurate Chemical & Scientific Corporation, catalog no. OBT0030; originally derived as an anti-BrdU antibody that is known to have strong reactivity toward CldU and very low reactivity toward IdU). Sections were incubated overnight with gentle shaking. Next day the solution of the anti-CldU antibody was replaced with a new mixture of primary antibodies. This new mixture contained rat monoclonal anti-CldU antibody and mouse monoclonal anti-IdU antibody (clone B44, BD Biosciences, catalog no. 347580; originally derived as an anti-BrdU antibody that is known to have strong reactivity toward IdU and very low reactivity toward CldU), both at a dilution 1:1,000, with 5% normal goat serum in PBST. When Nestin-GFP mice were examined, chicken polyclonal anti-GFP antibody (Aves Labs, catalog no. GFP-1020) at a dilution 1:400 was added to the mixture. Sections were incubated for additional 24 hr with gentle shaking.

After three washings with PBST, sections were incubated in the solution of secondary goat anti-rat IgG (H+L) antibody conjugated with ether Alexa 488 (Life Technologies, 1:500) in the case of C57BL/6 mice or DyLight405 (Jackson ImmunoResearch, 1:400) in the case of Nestin-GFP transgenic mice in PBST for 2 hr with gentle shaking. Then, the solution was replaced with a new mixture of secondary antibodies containing goat anti-rat IgG (H+L) antibody conjugated with Alexa 488 (1:500) and goat anti-mouse IgG (H+L) antibody conjugated with Alexa 633 (Life Technologies, 1:500) in the case of C57BL/6 mice or goat anti-rat IgG (H+L) antibody conjugated with DyLight405 (1:400), goat anti-chicken IgY (H+L) Alexa 488 (Life Technologies, 1:500), and goat anti-mouse IgG (H+L) antibody conjugated with Alexa 647 (Life Technologies, 1:1000) in the case of Nestin-GFP transgenic mice. All secondary antibodies were diluted in PBST. Sections were incubated for an additional 2 hr with gentle shaking followed by three washings in PBS. Free-floating brain sections were placed on gelatinized glass slides. All preparations were mounted with fluorescent mounting medium (DAKO) and coverslipped.

Note that in each case we used secondary antibodies against rat and mouse IgGs, which were also cross-adsorbed to mouse and rat IgGs, respectively, to reduce the unwanted secondary antibody cross-reaction.

A full protocol of the staining is presented in Figure S1. A modified protocol (for details see Figure S2) was applied to the brain and intestine sections co-stained with the antibody against Ki67.

Confocal Microscopy

Specificity of concurrent detection of three thymidine analogs was examined by conventional (by channels) and spectral imaging (for details see Supplemental Experimental Procedures) using

a Leica SP5 confocal platform (Leica Microsystems). To perform quantitative analysis of labeled cells, images of whole DGs were captured using a PerkinElmer spinning disk confocal microscope (PerkinElmer).

Cell Counting

Counting of labeled cells within the SGZ of the DG was performed manually on the images obtained with a complete series of 50 μm sections positioned 300 μm apart. The numbers obtained were extrapolated to the entire DG (Encinas and Enikolopov, 2008; Encinas et al., 2011). Quantitative data are presented as mean ± SEM.

Statistical Analysis

Statistical analysis was performed using GraphPad InStat software. Normality of the numbers of cells incorporating different labels or their combinations was assessed using the Kolmogorov-Smirnov test. One-way ANOVA followed by a Tukey-Kramer post hoc comparison was used to determine significance among subpopulations of cells that have incorporated different labels or their combinations.

Linear regression analysis of the cell fractions remaining in the S phase at the time of IdU injection was performed by determination of the Pearson correlation coefficient ($|R|$). The least-squares fit was applied to calculate the slope (m) and intercept (b) for an equation of the straight line ($y = mx + b$) for each animal. Then, the x-axis intercept corresponding to the duration of the S phase was determined. The estimation of the duration of the S phase is presented as mean value and SEM.

SUPPLEMENTAL INFORMATION

Supplemental Information includes Supplemental Experimental Procedures and three figures and can be found with this article online at https://doi.org/10.1016/j.stemcr.2017.12.020.

AUTHOR CONTRIBUTIONS

O.P. and G.E. designed the study; O.P. and N.P. performed the experiments; O.P., N.P., and G.E. analyzed the data; J.H.P. contributed to the critical early stages of the project; O.P. and G.E. wrote the manuscript.

ACKNOWLEDGMENTS

We thank Tatyana Michurina for help with experiments and valuable discussions. Part of the experiments were performed at the Core Center of the Koltzov Institute of Developmental Biology, Russian Academy of Sciences, Moscow. This work was supported by grants from the National Institute of Mental Health (R01MH092928), the National Institute on Aging (R01AG040209), the Russian Ministry of Education and Science (11.G34.31.0071), the Russian Science Foundation (grant 16-15-00294), and New York State Stem Cell Science (NYSTEM) (C029569) to G.E.

Received: June 17, 2017
Revised: December 21, 2017
Accepted: December 22, 2017
Published: January 18, 2018

REFERENCES

Bakker, P.J., Stap, J., Tukker, C.J., van Oven, C.H., Veenhof, C.H., and Aten, J. (1991). An indirect immunofluorescence double staining procedure for the simultaneous flow cytometric measurement of iodo- and chlorodeoxyuridine incorporated into DNA. Cytometry *12*, 366–372.

Clevers, H. (2013). The intestinal crypt, a prototype stem cell compartment. Cell *154*, 274–284.

Encinas, J.M., and Enikolopov, G. (2008). Identifying and quantitating neural stem and progenitor cells in the adult brain. Methods Cell Biol. *85*, 243–272.

Encinas, J.M., Michurina, T.V., Peunova, N., Park, J.H., Tordo, J., Peterson, D.A., Fishell, G., Koulakov, A., and Enikolopov, G. (2011). Division-coupled astrocytic differentiation and age-related depletion of neural stem cells in the adult hippocampus. Cell Stem Cell *8*, 566–579.

Gratzner, H.G. (1982). Monoclonal antibody to 5-bromo- and 5-iododeoxyuridine: a new reagent for detection of DNA replication. Science *218*, 474–475.

Griswold, M.D. (2016). Spermatogenesis: the commitment to meiosis. Physiol. Rev. *96*, 1–17.

Hayes, N.L., and Nowakowski, R.S. (2002). Dynamics of cell proliferation in the adult dentate gyrus of two inbred strains of mice. Brain Res. Dev. Brain Res. *134*, 77–85.

Hughes, W.L., Bond, V.P., Brecher, G., Cronkite, E.P., Painter, R.B., Quastler, H., and Sherman, F.G. (1958). Cellular proliferation in the mouse as revealed by autoradiography with tritiated thymidine. Proc. Natl. Acad. Sci. USA *44*, 476–483.

Kohlmeier, F., Maya-Mendoza, A., and Jackson, D.A. (2013). EdU induces DNA damage response and cell death in mESC in culture. Chromosome Res. *21*, 87–100.

Kulkarni, S., Micci, M.A., Leser, J., Shin, C., Tang, S.C., Fu, Y.Y., Liu, L., Li, Q., Saha, M., Li, C., et al. (2017). Adult enteric nervous system in health is maintained by a dynamic balance between neuronal apoptosis and neurogenesis. Proc. Natl. Acad. Sci. USA *114*, E3709–E3718.

Liboska, R., Ligasova, A., Strunin, D., Rosenberg, I., and Koberna, K. (2012). Most anti-BrdU antibodies react with 2′-deoxy-5-ethynyluridine – the method for the effective suppression of this cross-reactivity. PLoS One *7*, e51679.

Mandyam, C.D., Harburg, G.C., and Eisch, A.J. (2007). Determination of key aspects of precursor cell proliferation, cell cycle length and kinetics in the adult mouse subgranular zone. Neuroscience *146*, 108–122.

Mignone, J.L., Kukekov, V., Chiang, A.S., Steindler, D., and Enikolopov, G. (2004). Neural stem and progenitor cells in nestin-GFP transgenic mice. J. Comp. Neurol. *469*, 311–324.

Nowakowski, R.S., Lewin, S.B., and Miller, M.W. (1989). Bromodeoxyuridine immunohistochemical determination of the lengths of the cell cycle and the DNA-synthetic phase for an anatomically defined population. J. Neurocytol. *18*, 311–318.

Oatley, J.M., and Brinster, R.L. (2012). The germline stem cell niche unit in mammalian testes. Physiol. Rev. *92*, 577–595.

Ponti, G., Obernier, K., Guinto, C., Jose, L., Bonfanti, L., and Alvarez-Buylla, A. (2013). Cell cycle and lineage progression of neural progenitors in the ventricular-subventricular zones of adult mice. Proc. Natl. Acad. Sci. USA *110*, E1045–E1054.

Salic, A., and Mitchison, T.J. (2008). A chemical method for fast and sensitive detection of DNA synthesis in vivo. Proc. Natl. Acad. Sci. USA *105*, 2415–2420.

Takahashi, T., Nowakowski, R.S., and Caviness, V.S., Jr. (1994). Mode of cell proliferation in the developing mouse neocortex. Proc. Natl. Acad. Sci. USA *91*, 375–379.

Takahashi, T., Nowakowski, R.S., and Caviness, V.S., Jr. (1995). The cell cycle of the pseudostratified ventricular epithelium of the embryonic murine cerebral wall. J. Neurosci. *15*, 6046–6057.

Takahashi, T., Nowakowski, R.S., and Caviness, V.S., Jr. (1996). The leaving or Q fraction of the murine cerebral proliferative epithelium: a general model of neocortical neuronogenesis. J. Neurosci. *16*, 6183–6196.

Treweek, J.B., and Gradinaru, V. (2016). Extracting structural and functional features of widely distributed biological circuits with single cell resolution via tissue clearing and delivery vectors. Curr. Opin. Biotechnol. *40*, 193–207.

Vega, C.J., and Peterson, D.A. (2005). Stem cell proliferative history in tissue revealed by temporal halogenated thymidine analog discrimination. Nat. Methods *2*, 167–169.

Yang, B., Treweek, J.B., Kulkarni, R.P., Deverman, B.E., Chen, C.K., Lubeck, E., Shah, S., Cai, L., and Gradinaru, V. (2014). Single-cell phenotyping within transparent intact tissue through whole-body clearing. Cell *158*, 945–958.